A Mechanistic Study of the Influence of Proton Transfer Processes on the Behavior of Thiol/Disulfide Redox Couples

Eiichi Shouji and Daniel A. Buttry*

Department of Chemistry, University of Wyoming, Laramie, Wyoming 82071-3838

Received: November 30, 1998; In Final Form: December 3, 1998

The mechanism of the oxidation of 2-mercapto-5-methyl-1,3,4-thiadiazole (McMT) to its disulfide dimer and its subsequent reduction has been examined with a combined approach employing experimental data and digital simulation. In order to elucidate the influence of proton transfers on these redox processes, special attention has been paid to the influence of various bases, including triethylamine, pyridine, 3-chloropyridine, lutidine and 2,6-di-*tert*-butylpyridine, and proton donors, including methanesulfonic acid and trifluoromethanesulfonic acid, on both the oxidation and reduction reactions. On the basis of detailed comparisons of the experimental data with simulations of several mechanistic models, it is found that proton transfer pathways have a pronounced influence on both the oxidative and reductive pathways. In particular, McMT oxidation is facilitated by a rapid bimolecular proton transfer from McMT to weak bases such as Py that produces $McMT^-$, the thiolate form, which is then oxidized. There is no such facilitation in the presence of the sterically hindered base 2,6-di-*tert*-butylpyridine, suggesting that the facilitation occurs through the formation of a discrete hydrogen-bonded complex. The overall kinetic scheme by which these redox processes proceed both in the presence and absence of proton transfer agents is discussed, especially with regard to the potential use of a related dithiolate compound as a cathode material in Li secondary batteries.

Introduction

The potential use of 2,5-dimercapto-1,3,4-thiadiazole (DMcT, see Scheme 1) as part of a composite cathode material for secondary lithium batteries[1] has prompted a flurry of both spectroscopic and electrochemical investigations of the redox processes of this compound and several of its derivatives.[1−7] A particularly interesting aspect of the behavior of DMcT is the apparent facilitation of its oxidative polymerization and reductive depolymerization by poly(aniline) (PAn).[1−7] In fact, the cathode materials that have been shown to have very attractive energy densities[1] and rapid charging characteristics[3] have been based on molecular level composites of DMcT and PAn, sometimes with other additives present.[3] This facilitation of the DMcT redox process comprises an important finding, because, even though the thermodynamics of thiol/disulfide redox processes are quite attractive from the perspective of lithium cathode materials, their kinetics are typically very slow at room temperature.[8] Thus, gaining an understanding of the mechanism by which PAn accelerates the DMcT redox transformations is likely to be very worthwhile. While the mechanism of this facilitation has yet to be elucidated, previous results have suggested that proton transfer processes can have a strong influence on both the kinetics and thermodynamics of the thiol/disulfide redox couple.[7] In order to explore this issue in more detail, we have begun a detailed series of studies of the redox chemistry of thiadazole systems bearing thiol substituents in the presence of various acidic and basic proton transfer agents.[7] Given that oxidation of the dithiol systems, such as DMcT, results in polymerization and precipitation on the electrode surface, which leads to "phase-like" behavior and consequent deviations of the redox responses from theoretical expectations,[9−11] we have chosen to study the behavior of 2-mercapto-5-methyl-1,3,4-thiadiazole (McMT, see Scheme 1) as a model system,

SCHEME 1

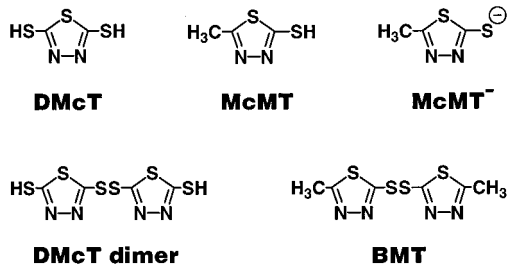

which has been briefly examined previously.[4,5,7] As will be seen below, this compound is oxidized to give a disulfide dimer in a well-behaved, quasi-reversible redox process. Thus, it provides a suitable couple for detailed comparison of experimental data with the results of digital simulations.

In constructing a kinetic scheme that satisfactorily describes the influence of proton-accepting bases on the redox behavior of McMT, it has been necessary to provide several thermodynamic and kinetic parameters as inputs for the digital simulation. As far as possible, these parameters have been obtained from a thorough survey of the literature. For example, an important reaction in the simulation is the coupling reaction of two $RS^•$ radicals to produce the RSSR disulfide species. This type of reaction has been studied previously,[12,13] and the rate constant has been found to be large. Thus, as will be seen below, a value of 10^6 M^{-1} s^{-1} was used in the simulation. Another reaction whose kinetics have a strong influence on the simulation is the reduction and subsequent cleavage of the SS bond in the disulfide dimer. In this case, spectral observations[12,13] of the $RSSR^{•-}$ intermediate, which decomposes to RS^- and $RS^•$, verify that the reduction occurs via a stepwise, rather than concerted, pathway,[14] and that the rate constant for the heterolytic

10.1021/jp984591f CCC: $18.00
Published on Web 03/06/1999

dissociative cleavage of $RSSR^{\bullet -}$ is $>10^5\ s^{-1}$. For this process, a value of $10^7\ s^{-1}$ was used in the simulation. For cases in which acid-base chemistry is important, values of pK_a for the various species in nonaqueous solvent systems have been used wherever possible.[15−20] In particular, a well-established correlation[20] between the pK_a of radical cations of thiol species, the pK_a of the parent thiol, and the difference in oxidation peak potential for the thiolate anion and the thiol has been used to estimate the pK_a of the radical cation of McMT. Finally, since proton transfer to and from heteroatoms and heteroatomic cation radicals is typically quite fast,[21,22] fairly large values for the rate constants for such proton transfer reactions were used. We will return to a more thorough discussion of the various kinetic and thermodynamic values used as inputs for the simulation below.

An additional consideration about the use of simulations to model such processes relates to the fact that the simulation requires that the redox processes be treated as a series of elementary steps. Thus, for example, in the reduction of a species such as RSSR, each of the two electron transfers that ultimately will produce 2 equiv of RS^- must be expressed and calculated separately within the simulation, along with any intermediate chemical reactions that are thought to occur along the reaction pathway. In many cases, the sequence of elementary steps used in the simulation can be combined in a thermodynamic cycle[20,23,24] to construct the overall reaction. For example, for RSSR reduction the overall reaction would be

$$RSSR + 2e^- \rightarrow 2\ RS^- \qquad (1)$$

while the elementary steps would involve reduction of RSSR by one electron, its subsequent dissociation to give RS^- and $RS^{\bullet}$, and the subsequent reduction of the radical to give RS^- or its dimerization to give RSSR, which will itself be reduced, etc. Because these elementary steps are thermodynamically interrelated, their equilibrium constants (for chemical reactions) and $E°$ values (for electrochemical reactions) cannot be varied independently, providing some constraints on the number of independent variables in the simulation. It is important to note that these thermodynamic constraints are included in the determination of the values used in these simulations described below.

Experimental Section

Materials. Acetonitrile (AN) was purchased from Aldrich Chemical Inc., purified by distillation from P_2O_5, and stored over 3 Å molecular sieves. These procedures produce adventitious water concentrations below 1 mM. This, coupled with the fact that all electrochemical experiments were carried out with 10 mM concentrations of the various redox compounds, strongly suggests that any possible influences of water as a proton source or sink can be discounted. McMT was purchased from Aldrich and was used after recrystallization from AN. 3-Chloropyridine, pyridine, lutidine, 2,6-di-*tert*-butylpyridine, and triethylamine were also purchased from Aldrich Chemical Inc. and were used after purification by distillation. Deuterated acetonitrile (AN-d_3) for NMR measurements was used as purchased from Aldrich.

Electrochemical Measurements. Cyclic voltammograms were obtained at 25 °C using a BAS CV-27 and a Hewlett-Packard 7045B *xy* recorder. Measurements were taken in a three electrode cell configuration using a glassy carbon disk electrode (Cypress Systems, Inc., 3.0-mm diameter), a Pt coil (0.5-mm diameter, 50-cm length), and a Ag/AgCl reference electrode, against which all potentials are reported. Unless otherwise noted, all experiments were conducted in a 0.2 M $LiClO_4$ AN solution, which was extensively deaerated using nitrogen gas, and at a scan rate of 50 mV s^{-1}.

Spectroscopic Methods. UV−vis spectra were recorded using a Hewlett-Packard HP8452 diode array spectrometer in AN solution. IR spectra in AN solution were recorded using a Bomem MB100 spectrometer (MCT detector, resolution of 1 cm^{-1}) in AN solution with the solution placed between two KBr crystals (25-mm diameter, 5-mm thickness). Raman spectra were recorded using a Spectra-Physics Stabilite 2017 Ar ion laser (514.5 nm) and a SPEX 270M single monochromator with a Spectrum One CCD detector. NMR spectra were recorded using a JEOL NMR-270 MHz in AN-d_3 solution. Considerable care was taken to ensure the exclusion of both oxygen and water from the samples during these experiments.

Digital Simulations. Simulations of cyclic voltammograms[23] were done using Digisim Ver. 2.1 (Bioanalytical Systems, Inc.) with a personal computer (Pentium 200MHz Pro, Windows95). The following model parameters were used: exponential grid factor 0.5; potential step 5×10^{-3} V, noise level 0 A; temperature 25 °C; scan rate 50 mV s^{-1}; diffusion coefficient 1×10^{-5} cm^2/s. Pre-equilibrium was enabled for chemical reactions only. To verify that the simulation results did not depend on increases in the resolution of the simulation, the grid factor was varied from 0.5 to 0.1, and the potential step was varied from 5 to 1 mV. None of these variations led to discernible changes in the simulated cyclic voltammograms, although the calculations became extremely lengthy. Diffusion coefficients were all assigned values of 1×10^{-5} cm^2/s, even though it is likely that some values were substantially different from this (e.g., the H^+ diffusion coefficient is probably considerably larger than that for the much larger BMT species). Because the simulations couple the rate constants with the diffusion coefficients to produce dimensionless parameters, this produces small errors in the rate constants generated from the simulations. However, since the motivation of the study was to understand qualitatively the influence of protons on the voltammetry of the McMT thiol/disulfide redox couple, this is not a serious concern.

Results and Discussion

Redox Behavior of the Disulfide Dimer. Scheme 1 shows the structures of McMT, its thiolate form ($McMT^-$), and the disulfide dimer (BMT) that is formed by oxidation of either one of these species. Simulation of the McMT/BMT system is complicated by the acid−base and other chemistry that can follow the redox processes. For example, McMT oxidation produces the radical cation species $McMT^+$, which can deprotonate, producing the $McMT^{\bullet}$ radical which can then dimerize via radical−radical coupling. On the other hand, reduction of BMT initially produces $BMT^{\bullet -}$, which will dissociate to produce $McMT^-$ and $McMT^{\bullet}$, which itself can either be reduced to $McMT^-$ or dimerize with another $McMT^{\bullet}$ to generate more dimer, followed by its reduction, etc. Thus, the overall mechanisms of these redox transformations involve several reactions, some of which are thermodynamically related (see below). In order to minimize the number of independent variables initially employed in the simulations, we begin by examining the simplest redox process: reduction of BMT to ultimately produce $McMT^-$ and its subsequent reoxidation back to BMT. As will be seen, this transformation can be treated using a set of four

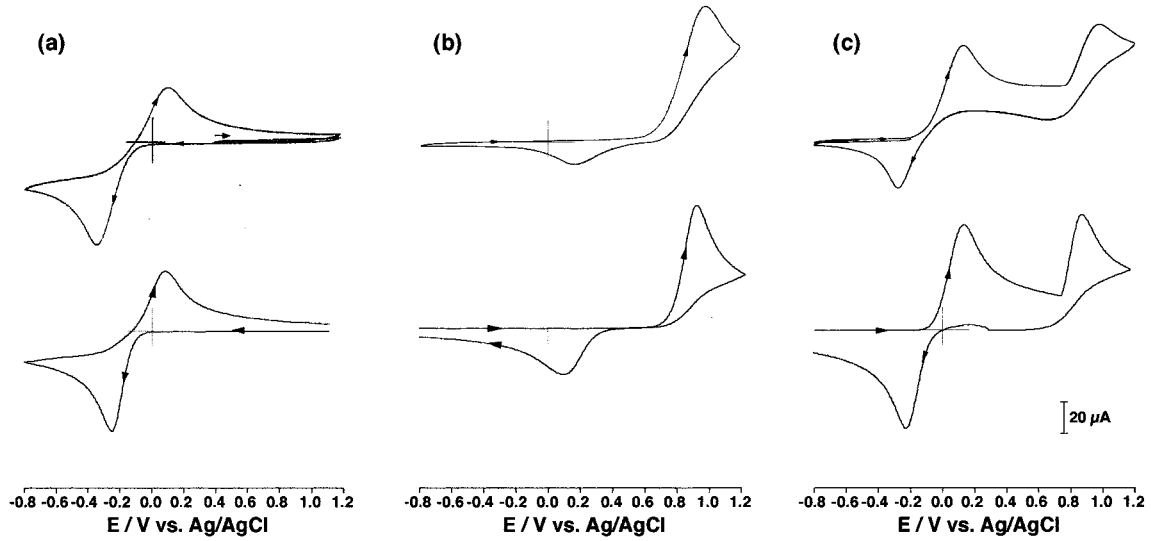

Figure 1. Experimental (upper) and simulated (lower) cyclic voltammograms for (a) 10 mM BMT with initial scan in positive direction from 0.3 V, (b) 10 mM DMcT with initial scan negative from 0.0 V, and (c) 10 mM McMT + 5 mM TEA with initial scan negative from −0.3 V.

TABLE 1. Simulation Parameters for Pyridine

no.	electrochemical reactions	$E°$/V	k_s/cm s
1e	$McMT^{\bullet+} + e^- \leftrightarrow McMT$	0.80	5×10^{-4}
2e	$McMT^{\bullet} + e^- \leftrightarrow McMT^-$	0.09	2×10^{-3}
3e	$dimer + e^- \leftrightarrow dimer^{\bullet-}$	−0.32	5×10^{-2}
4e	$dimer\text{-}H^+ + e^- \leftrightarrow dimer^{\bullet}\text{-}H$	0.33	3×10^{-4}

no.	chemical reactions	K_{eq}	k_f
1c	$dimer^{\bullet-} \rightleftarrows McMT^{\bullet} + McMT^-$	1×10^0	1×10^7 [a]
2c	$McMT^- + H^+ \rightleftarrows McMT$	1×10^{12} [c]	1×10^{11} [b]
3c	$2McMT^{\bullet} \rightleftarrows dimer$	1×10^7	1×10^7 [a]
4c	$McMT^{\bullet+} \rightleftarrows McMT^{\bullet} + H^+$	1×10^0	1×10^5 [b]
5c	$dimer + H^+ \rightleftarrows dimer\text{-}H^+$	5×10^{-1}	1×10^{10}
6c	$dimer^{\bullet}\text{-}H \rightleftarrows McMT^{\bullet} + McMT$	1×10^{-1}	1×10^8
7c	$base + H^+ \rightleftarrows base^+\text{-}H$	5×10^7 [d]	1×10^8 [b]
8c	$base + McMT \rightleftarrows McMT^- + base^+\text{-}H$	5×10^{-5} [e]	2×10^7
9c	$base + McMT^{\bullet+} \rightleftarrows McMT^{\bullet} + base^+\text{-}H$	5×10^7 [e]	1×10^9

[a] References 12 and 13. [b] Reference 12. [c] This values was considered using pK_a of triethylamine and pyridine with refs 14 and 21. [d] 3×10^6 for 3-chloropyridine, 5×10^{16} for triethylamine cases. [e] Thermodynamically superfluous reactions (TSRs, ref 24).

equations, three of which are independent. After using the simulation to fit this simple case, we will increase the level of complexity by including the proton transfer reactions necessary to model the reactions involving acids and bases. It is important to note here that the simulations for the more complex cases will be done *with no changes to the values used for the simpler cases.* Thus, this approach represents a sort of *aufbau* method for building up a simulation; the values for the simpler cases are required also to fit the more complex cases without adjustment.

Figure 1a shows a cyclic voltammogram (CV) of a 10 mM solution of BMT. The upper curve, which gives the experimental result, shows a reduction peak at ca. −0.4 V and a corresponding oxidation peak at ca. 0.0 V. These correspond to the reduction of BMT to give 2 equiv of $McMT^-$ and the subsequent oxidation of $McMT^-$ back to BMT, respectively. The lower curve gives the simulated result for this case. The elementary reactions required to generate this CV are shown in Table 1 and comprise reactions 2e, 3e, 1c, and 3c. The redox potentials, equilibrium constants and rate constants used to produce the simulated curve are as shown. Note that these four equations are connected by the following relationship, which derives from the Nernst equation and the appropriate equilibrium expressions

$$(K_{1c}K_{3c})^{-1} = \exp[(nF/RT)(E_{3e} - E_{2e})] = [BMT^{\bullet-}][McMT^{\bullet}]/[BMT][McMT^{\bullet-}] \quad (2)$$

where $n = 1$ electron, $F = 96485$ C mol^{-1}, and the other quantities have their usual meaning. Thus, only three of these equations are independent. Feldberg and co-workers have discussed the methods by which such thermodynamically superfluous reactions (TSRs) are identified and properly constrained within the simulation.[24]

It is evident from the figure that the simulation reasonably reproduces the essential features of the experimental data. The values provided in the table for reactions 2e, 3e, 1c and 3c produce an acceptable fit to the experimental CV. Other possible combinations of parameters can also provide acceptable fits to this simple case. However, as will be seen below, while these other combinations cannot be simultaneously used to fit more complex situations, the same kinetic and thermodynamic parameters shown in Table 1 for reactions 2e, 3e, 1c, and 3c can be used as part of the fit for the more complex cases involving proton transfer, so long as the appropriate acid−base reactions are included.

Note that the simulation requires two, separate redox processes to reproduce the CV. One is the $McMT^-$/McMT redox couple, and the other is the $BMT/BMT^{\bullet-}$ redox couple. It is sensible that different $E°$ are used for each of these, since the redox potentials for these two couples should be related to the HOMO of $McMT^-$ and the LUMO of BMT. This general approach is consistent with many previous studies of the relationship between $E°$ and molecular orbital energies.[25] Of course, the peak positions in the CV are also influenced by the rates of the chemical reactions that follow the initial electron transfer event and by the heterogeneous electron transfer rate constants (k_s values), as given in Table 1.

An important test of any simulation involves examining the agreement between theory and experiment over a range of time scales. In the present case, this is accomplished by simulating the CV at a variety of scan rates. Figure 2 shows experimental (upper) and simulated (lower) voltammograms for BMT reduction at scan rates from 25 to 400 mV s^{-1}, a range representing more than an order of magnitude change in time scale. As can

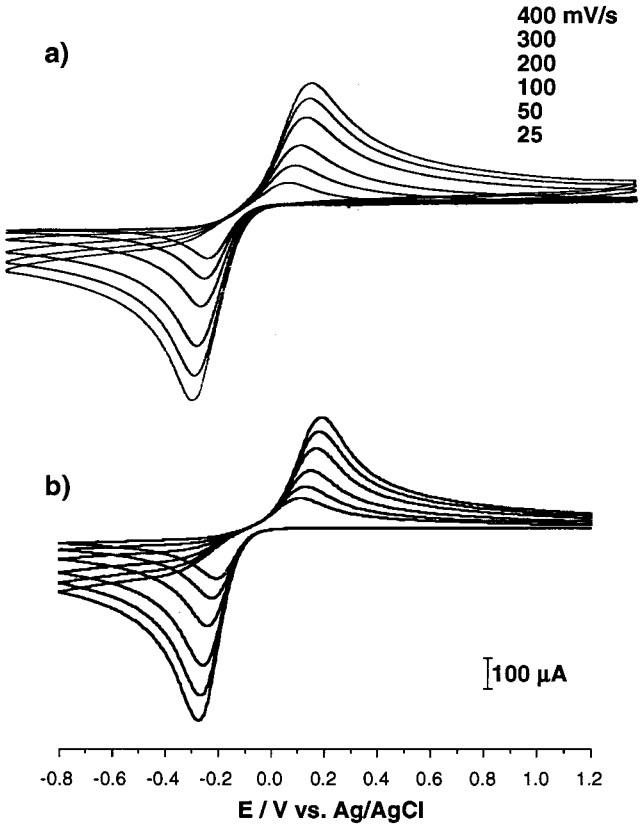

Figure 2. Experimental (upper) and simulated (lower) cyclic voltammograms for a 10 mM BMT solution with initial scan in negative direction from 1.2 V. Scans are shown for scan rates of 25, 50, 100, 200, 300, and 400 mV s^{-1}.

be seen, the agreement between theory and experiment is excellent over the entire range, strongly suggesting that the simulation is capturing the essential features of the kinetic and thermodynamic processes that manifest in the experimental voltammogram.

Redox Behavior of McMT and McMT$^-$. Figure 1b shows the experimental (upper) and simulated (lower) cyclic voltammograms for McMT oxidation. As can be seen, McMT is oxidized with a peak potential at +0.95 V, producing an oxidized product that is subsequently reduced at ca. 0.1 V. Previous work has shown that this oxidation produces the disulfide dimer, BMT, (see Scheme 1) and that reduction of the dimer regenerates the thiol.[4,5] We have recently obtained a crystal structure of BMT that unambiguously verifies it as the product of the oxidation.[26] Note that, under the conditions in Figure 1b, protons are released to the AN solution as a consequence of the oxidation. Comparison of the peak potentials for reduction of the BMT disulfide dimer in the experimental curves in Figure 1a (−0.35 V) and b (0.1 V) reveals that the availability of these protons strongly influences the potential of this reduction process.

Successful simulation of the McMT redox process requires that several additional reactions be included in the model. These are given in Table 1 and comprise: 1e, which describes the oxidation of McMT to McMT$^{\bullet+}$; 4c, which describes deprotonation of McMT$^{\bullet+}$ to produce a "free" proton and McMT$^\bullet$ radical; 5c, which describes a rapid pre-equilibrium that produces small amounts of protonated BMT; 4e, which describes the reduction of this protonated dimer; 6c, which describes the rapid heterolytic cleavage of the reduced, protonated dimer to give McMT$^\bullet$ radical and McMT; and 2c, which describes the protonation of McMT$^-$ to regenerate McMT. It should be particularly noted that reactions 4e, 5c, and 6c were essential to successfully simulating the experimental CV. Various mechanisms using other reactions were investigated, but with no success. Specifically, one such mechanism that was exhaustively investigated involved rapid protonation of the reduced dimer (i.e. $H^+ + BMT^{\bullet-} \rightarrow HBMT$) followed by rapid cleavage of this species to give McMT and McMT$^\bullet$. Under no circumstances was it possible to simultaneously produce acceptable fits for the CVs in Figure 1a and b using a mechanism of this type.

This pre-equilibrium protonation prior to the reduction of the BMT dimer is conceptually quite similar to the square schemes that are used to describe the reduction of systems such as benzoquinone in the absence and presence of proton donors.[27] As is the case here, the reduction is facilitated by a proton transfer to the electron acceptor prior to the reduction step. Further, the change in redox potential that occurs on protonation is similar in the present case and that of benzoquinone[27] ($E°$ for quinone reduction shifts ca. 0.5−0.9 V less negative on protonation, depending on conditions). Thus, the use of reaction 4e is well precedented in the literature concerning the influence of proton donors on reduction potentials.

One feature of the CV for McMT that is less well fit than the others is the intensity of the return peak (i.e. reduction of BMT in the presence of protons) following McMT oxidation. Specifically, the experimental peak current is typically only 50−60% of that predicted by the simulation. The origins of this effect are uncertain, but it seems most likely to be due to one or more parasitic side reactions of the McMT$^\bullet$ radical species produced during the oxidation. However, since the primary motivation for the study was to understand the influence of proton transfer processes on the thiol/disulfide redox transformations, we would argue that this deficiency of the simulation is of only minor concern.

To further examine the proton-facilitated reduction pathway represented by reactions 4e, 5c, and 6c we examined the influence of strong proton donors on the reduction of BMT. Figure 3 shows the voltammetry that is observed for BMT in the presence of trifluoromethanesulfonic acid (TFA), a very strong acid. As TFA is successively added to the solution, one observes an increase in the proton-facilitated reduction wave at ca. 0.1 V. For molar ratios of TFA/BMT less than 2, this increase is directly proportional to the TFA concentration. In addition, after traversing this reduction wave, one also observes a new oxidation process at 0.85 V that is characteristic of McMT oxidation (see Figure 1b). This is as expected, since BMT reduction in the presence of protons will produce McMT. Note that the initial scan in all of these cases was in the positive direction, showing that McMT is produced only after BMT reduction in the presence of H^+. Figure 4 shows the simulation of these cases, in which addition of TFA is modeled by introducing "free" H^+ into the solution prior to the voltammetry. It is significant that none of the kinetic or thermodynamic parameters that were used for simulating the McMT case have been changed. As can be seen, the agreement between the experimental data and the simulation is quite good, arguing for the validity of the reduction pathway embodied in reactions 5c, 4e, and 6c in Table 1.

As a further test of the mechanism used in the simulation of the McMT redox system, the influence of addition of a strong base to a solution of McMT was examined. Figure 1c shows the result of addition of one-half molar equivalent of triethylamine, TEA, to a solution of McMT prior to the voltammetric experiment. On the basis of the aqueous pK_a values for TEA[28] and McMT[4] of 10.7 and 5.35, respectively, as well as the results

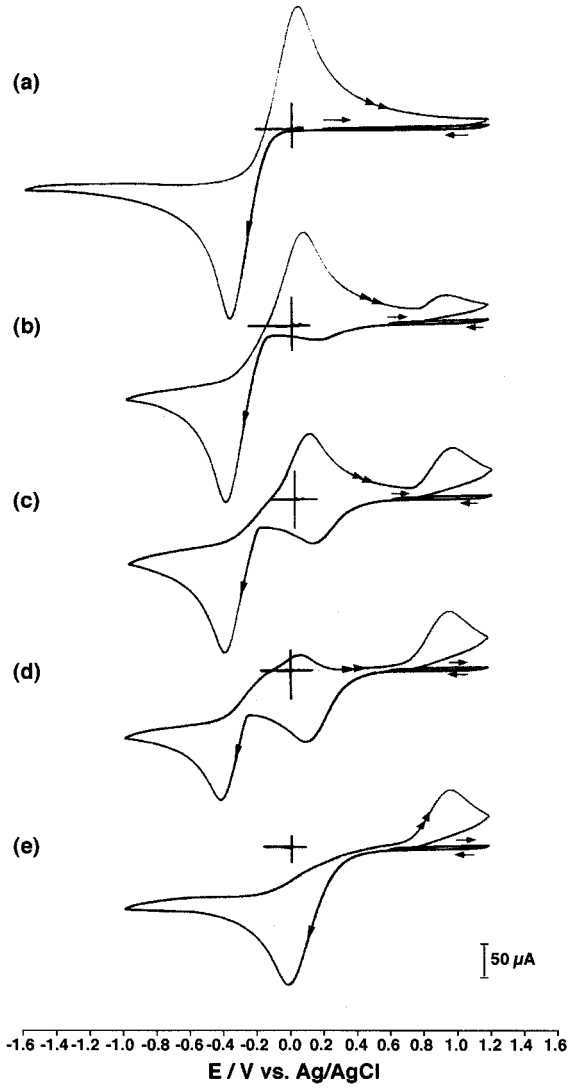

Figure 3. Experimental cyclic voltammograms for 10 mM BMT in solutions containing (a) no TFA, (b) 2 mM TFA, (c) 5 mM TFA, (d) 10 mM TFA, and (e) 20 mM TFA. The initial scan in a is positive from 0.0 V and in all others positive from 0.5 V.

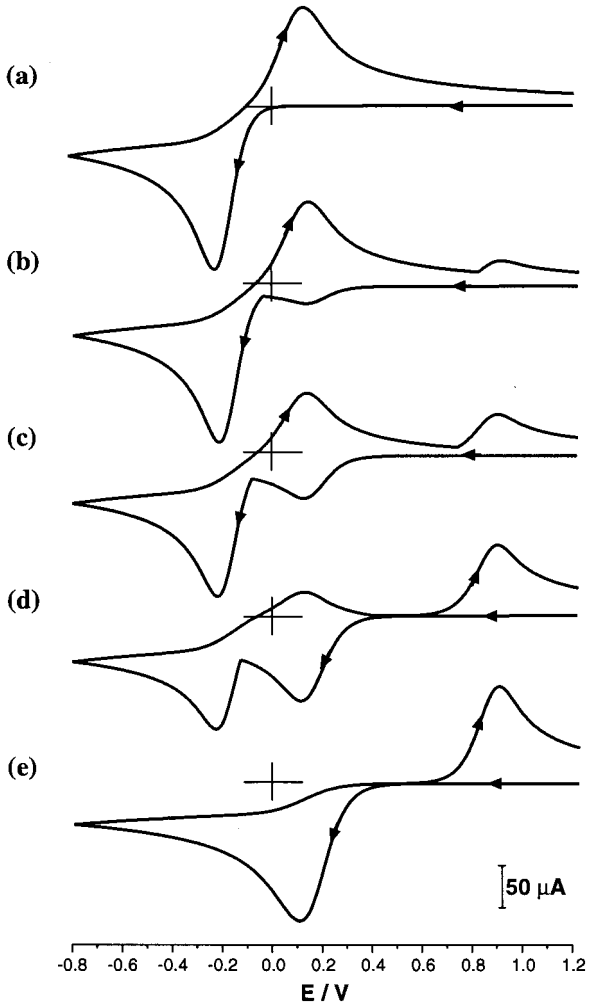

Figure 4. Simulated cyclic voltammograms for 10 mM BMT in solutions containing (a) no TFA, (b) 2 mM TFA, (c) 5 mM TFA, (d) 10 mM TFA, and (e) 20 mM TFA. All conditions as in Figure 2, except that initial scan directions are all negative starting from 1.2 V.

of previous experiments,[7] one expects that TEA should fully deprotonate 50% of the McMT, in this case producing a solution that is 5 mM in McMT and 5 mM in $McMT^-$. The experimental CV (upper curve) shows a redox response characteristic of a 5 mM solution of $McMT^-$ (i.e., the BMT/$McMT^-$ redox couple, as in Figure 1a) centered at ca. −0.1 V, as well as the oxidation of the remaining 5 mM McMT, in accord with expectations. It is interesting that no reduction peak at 0.1 V for the proton-facilitated reduction of the BMT disulfide dimer is observed when the molar ratio of TEA/McMT is greater than or equal to 0.5. This is because the protons that are produced by McMT oxidation are rapidly consumed by protonation of $McMT^-$ that is arriving by diffusion from solution. Thus, the proton-facilitated pathway for reduction of the dimer at 0.1 V is not available.

The simulation of the TEA case is shown in Figure 1c (lower curve). Successful simulation of this case required the inclusion of reaction 7c, which describes the protonation reaction for the base. The K_{eq} value for this reaction was assigned a value of 10^{16}, which is sufficient to cause McMT to protonate essentially all of the TEA that is present, provided the TEA/McMT ratio is less than 1. Note that the elimination of the proton-facilitated reduction peak at 0.1 V when TEA/McMT > 0.5 is successfully modeled by the simulation. The voltammetric responses for several other experimentally examined molar ratios of TEA/McMT were also successfully modeled using the same set of simulation parameters.

Before proceeding with a description of the influence of weak bases on the redox behavior of McMT, it is worth briefly discussing the significance of the pK_a values that are used in the simulation. Since the experiments were done in AN solution, these values are referenced with respect to the stability of the proton in AN.[15] The pK_a values used in the simulation for the conjugate acids of TEA and the pyridine bases (see below) have been chosen based on previously reported values in AN, DMSO and other nonaqueous solvents[15,18,29,30] and are assigned the following pK_a values in AN: TEA (16), lutidine (10), pyridine (8.7), 2,6-di-*tert*-butylpyridine (8.7), and 3-chloropyridine (7.5). On the basis of a previous experimental observation[7] that, for this series of bases in AN solution, McMT is deprotonated only by TEA, McMT has been assigned a pK_a of 13 in the simulation, midway between the TEA and lutidine values. In contrast, some of the species required for the mechanism employed in the simulation are very strongly acidic. For example, reactions 4c and 5c refer to protonation reactions in which very weak bases ($McMT^•$ and BMT, respectively) are partially protonated by "free" protons in AN. However, these free protons are actually solvated by acetonitrile. Thus, pK_a values of 1 and -0.3 for $McMT^{•+}$ and $HBMT^+$, for reactions 4c and 5c, respectively,

imply that the conjugate bases of these species have basicities comparable to that of AN, which is ca. −10 on an aqueous scale.[28] In comparison, a pK_a value for McMT of 13 implies that it is ca. 12 orders of magnitude less acidic than its cation radical, McMT$^{\bullet+}$. Bordwell et al.[20] have discussed the relative acidities of thiols (pK_{HA})and their cation radicals (p$K_{HA\bullet+}$), and have proposed a correlation that can be used to critically examine the values that have been used in the present simulations. Briefly, they proposed the following relationship

$$pK_{HA\bullet+} = pK_{HA} + 16.8[E_{ox}(A^-) - E_{ox}(HA)] \qquad (3)$$

where $E_{ox}(A^-)$ and $E_{ox}(HA)$ are the oxidation peak potentials for the thiolate and thiol, respectively, which in the present case are McMT$^-$ and McMT. They used this correlation to estimate the pK_a values for the cation radicals of 15 thiol compounds. The results were found to be quite satisfactory, with an uncertainty of ca. ±2 pK_a units.[20] On the basis of the experimentally observed peak potentials for McMT$^-$ and McMT and the pK_a of McMT that was used in the simulation (13, see above), this relationship predicts that the pK_a of McMT$^{\bullet+}$ should be 1.3 (±2). This reasoning was used to assign a value of 1.0 to this species in the simulation. This discussion shows that the quantitative treatment of the acid−base chemistry of the various species in the simulation is both internally consistent and consistent with the existing literature.

Redox Behavior of McMT in the Presence of Weak Bases. Figure 5 shows the behavior that results when increasing amounts of pyridine are added to an AN solution containing McMT. One observes the appearance of a new oxidation peak at ca. +0.55 V and a corresponding reduction at ca. −0.3 V. These two new peaks shift slightly in the positive direction and increase in magnitude linearly with the concentration of pyridine up to the point at which it becomes equimolar with McMT, after which the voltammetry does not change significantly. Corresponding decreases in the peaks due to the McMT/McMT$^{\bullet+}$ redox couple are also observed. Note that the peak at 0.1 V for the proton-facilitated reduction of the dimer is not observed above a molar ratio of Py/McMT of 0.5, as was the case for TEA. As in the TEA case, this is caused by consumption of the free (AN-solvated) protons by protonation of Py that is supplied by diffusion from bulk solution.

Before discussing the preferred interpretation of these results, it should be pointed out that they are *not* consistent with stoichiometric deprotonation of McMT by pyridine (Py) to produce bulk McMT$^-$ prior to the redox process. This is made clear by comparison of Figure 5 with Figure 1a and c, which show the redox behavior of the McMT$^-$/BMT redox couple. The new response observed in the presence of Py is definitely not the same as that observed for the McMT$^-$/BMT redox couple. Further, previous UV−vis spectral studies have demonstrated that Py is not a sufficiently strong base to deprotonate McMT.[7] To corroborate these findings, NMR studies[31] of the McMT/Py system were conducted. Figure 6 shows the NMR spectra that are observed for solutions of McMT (curve a), Py (curve c), McMT/Py (curve b), and Py/MSA (curve d, in which the pyridinium cation is produced). Comparison of curves b and d shows that the pyridinium cation is not produced in solutions of McMT/Py, even when Py is present in molar excess. We have also used FTIR[32] and Raman[33] spectroscopies to examine this system. In all cases, solutions of McMT and Py were found to contain only the parent compounds; pyridinium could not be detected in any case. Similar experiments were also done to test for stoichiometric proton transfer between McMT and the other pyridine derivatives used in this study, and no evidence for stoichiometric deprotonation of McMT by any of them was observed. Thus, the voltammetric responses shown in Figure 5 are most definitely not due to bulk, stoichiometric production of McMT$^-$.

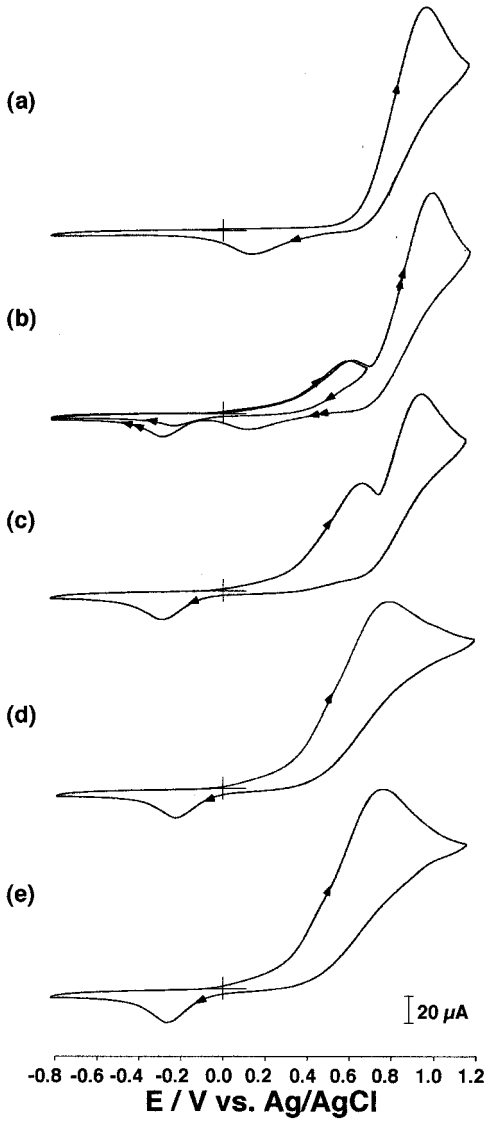

Figure 5. Experimental cyclic voltammograms for 10 mM McMT in solutions containing (a) no Py, (b) 2 mM Py, (c) 5 mM Py, (d) 10 mM Py, and (e) 20 mM Py. Initial scan directions are all positive from -0.8 V. In (b), an additional scan with a positive limit of 0.6 V is shown that demonstrates the response from only the Py, proton-transfer-facilitated process (see text).

Figure 7 shows the simulated CV for the same set of conditions as in Figure 5. Quite good agreement between the experimental data and the simulation is observed. Exhaustive tests of the simulation using a wide range of values for the various reactions showed that successful simulation of these cases required the inclusion of two additional reactions beyond those that have already been discussed. Specifically, reactions 8c and 9c must be included in order to achieve an acceptable agreement between the experimental data and the simulation. These reactions are TSR because the acidity and basicity of the proton donors and acceptors in these reactions are defined in reactions 2c, 4c, and 7c. Thus, the equilibrium constants for these reactions are not adjustable in the simulation. On the other hand, the rate behavior can be adjusted. On the basis of previous descriptions of rapid proton transfer in related systems,[21,22]

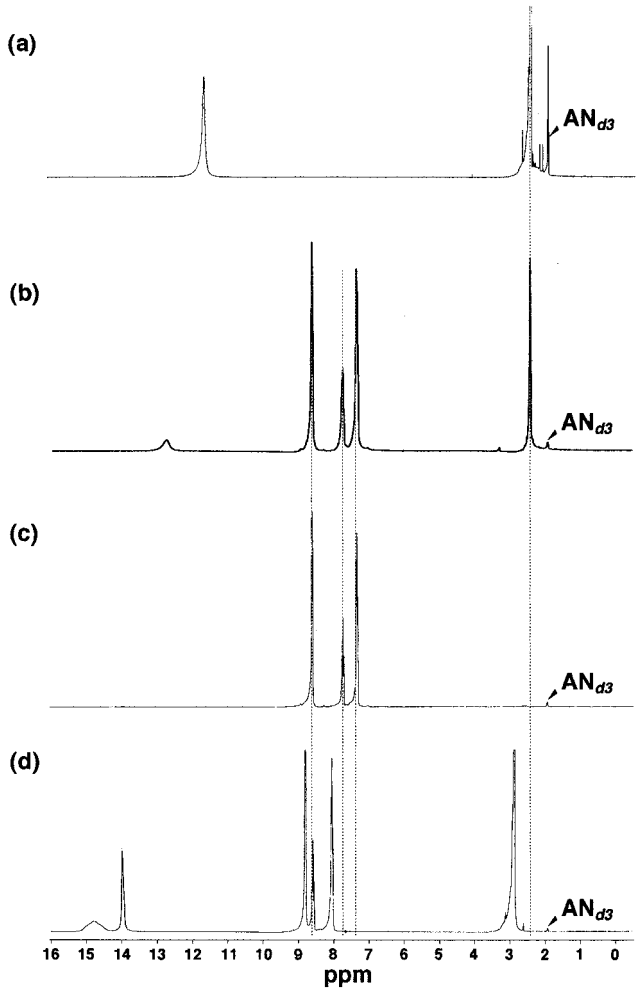

Figure 6. ^{1}H NMR spectra in AN-d_3 solution for 50 mM concentrations of (a) McMT alone, (b) McMT plus Py ([Py]/[McMT] = 2), (c) Py alone, and (d) McMT plus MSA ([MSA]/[McMT] = 2).

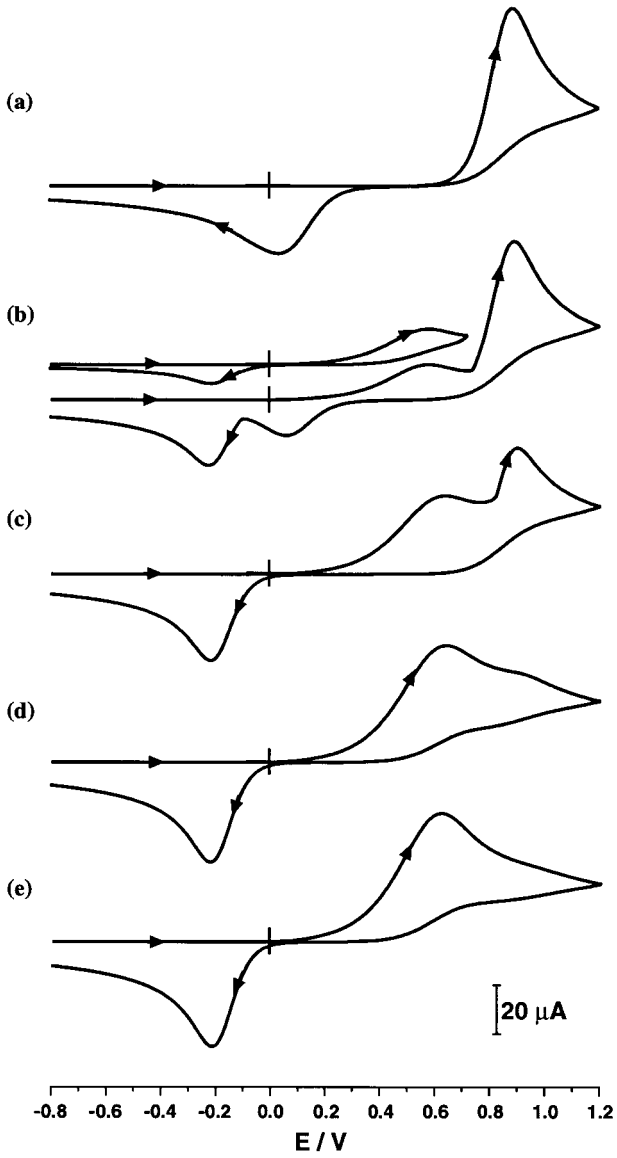

Figure 7. Simulated cyclic voltammograms for 10 mM McMT in solutions containing (a) no Py, (b) 2 mM Py, (c) 5 mM Py, (d) 10 mM Py, and (e) 20 mM Py. All conditions as in Figure 5 except that initial scan directions are all positive from −0.8 V. In b, an additional scan with a positive limit of 0.6 V is shown that demonstrates the response from only the Py, proton-transfer-facilitated process (see text).

relatively rapid proton exchange is assumed for these equilibria as reflected in the rate constants used in Table 1.

Detailed examination of the concentration profiles for the various species in the simulation reveals that the primary manner in which reactions 8c and 9c affect the simulation is by providing a rapid pathway through which $McMT^-$ can be produced. Thus, reaction 8c provides a rapid pathway for $McMT^-$ production, so that it can be oxidized at potentials less positive than those required for direct oxidation of McMT. Reactions 8c plus the reverse of 2e essentially represent a C_rE_i process (i.e., reversible chemical reaction followed by an irreversible electrochemical reaction) in the electrochemical notation.[34] In addition, reaction 9c drives the formation of $McMT^•$, which then couples rapidly to form BMT. Both processes contribute to the new peak at ca. 0.55 V, which is nearer the $McMT^-$ oxidation potential. In this case, the shape of the response is characteristic of a C_rE_i case in which the preceding chemical reaction is rapid enough to maintain equilibrium at the scan rate employed.[34] It is worth noting that the thermodynamically identical pathway comprising the reverse of reaction 2c (i.e., McMT dissociation to $McMT^- + H^+$) and reaction 7c (i.e., Py protonation) does not produce simulated results that fit the experimental data. This is because the "unassisted" dissociation of McMT is very unfavorable in AN solution. Thus, even though this overall process can produce sparing amounts of $McMT^-$ in a thermodynamic sense, it cannot produce them rapidly enough to lead to the new oxidation at 0.55 V, given reasonable values for the rate constants for reactions 2c and 7c. This suggests that the rapid production of $McMT^-$ that is responsible for the new peak at 0.55 V in Figures 5 and 7 is due to a true bimolecular process involving McMT and Py, perhaps involving a hydrogen-bonded complex along the reaction pathway (see below).

Several other pyridine derivatives exhibit similar abilities to facilitate the oxidation of McMT. This can be seen in Figure 8, curves a and b, which show the behavior in solutions of 3-chloropyridine and lutidine, respectively. It is significant that the position of the facilitated oxidation peak depends on the pK_a of the conjugate base of the pyridine derivative. This is physically reasonable, since less basic derivatives will not allow as rapid a production of $McMT^-$. Figure 9 shows simulations for the lutidine (curve a), pyridine (curve b) and 3-chloropyridine (curve c) cases. As can be seen by comparison to the data in Figures 5 and 8, the simulation produces very good agreement with the experimental data for these cases. Note that the forward rate constants for reactions 8c and 9c are not adjusted for these

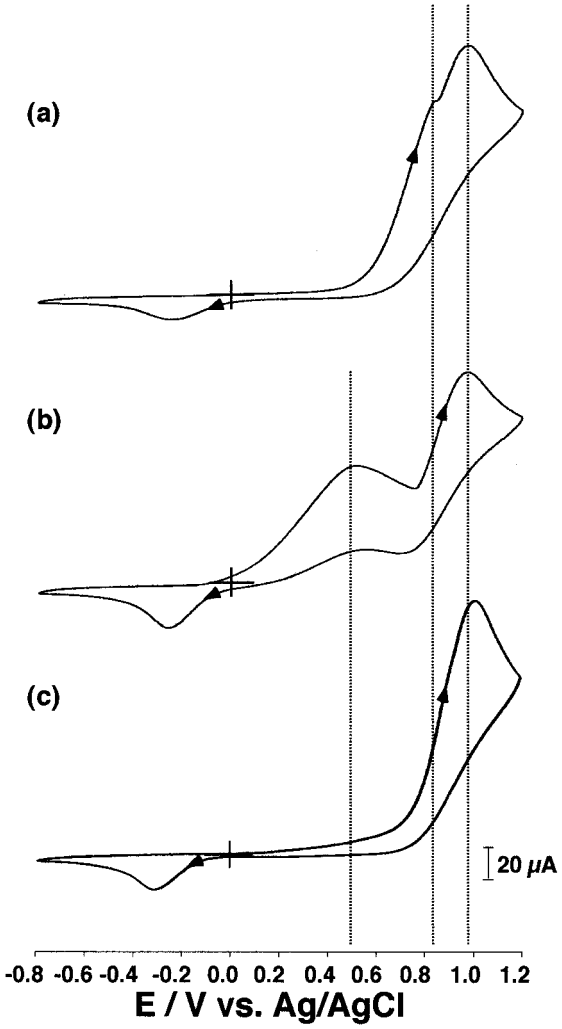

Figure 8. Experimental cyclic voltammograms for 10 mM solutions of McMT containing (a) 5 mM 3-chloropyridine, (b) 5 mM lutidine, and (c) 5 mM 2,6-di-*tert*-butylpyridine. Initial scan directions are all positive from -0.8 V.

simulations. Rather, the entire effect of changing the basicity of the pyridine derivative is embodied in changes in the equilibrium constant for reactions 8c and 9c for the different derivatives. Note also that, as discussed above, these reactions are TSRs. Their equilibrium constants are *not* independently adjustable, but rather are fixed by those for reactions 2c, 4c, and 7c. Thus, the mechanism used in the simulation is able to quantitatively fit the experimental results for a wide variety of bases using only changes in their pK_a values.

To further explore the possible involvement of bimolecular proton transfer in the facilitated oxidation of McMT by pyridine bases, the behavior of the sterically hindered base, 2,6-di-*tert*-butylpyridine, was examined. This base was chosen because the pK_a of its conjugate base is quite close to that of Py.[30,35] However, it has been reported previously that this base experiences severe steric hindrance in proton-transfer reactions.[21] Thus, it was expected that proton transfer from McMT to 2,6-di-*tert*-butylpyridine would be inhibited. In fact, as can be seen in Figure 8, curve c, this base has absolutely no effect on the oxidation of McMT. This important result makes clear the fact that these bases are not simply acting as buffer systems that provide thermodynamic sinks for the protons generated during McMT oxidation. Rather, in order to facilitate McMT oxidation they must be capable of a bimolecular proton transfer reaction with McMT, presumably through formation of a hydrogen bonded complex. Thus, reaction 8c does not fully describe the behavior under these conditions, because there must be an intermediate along the reaction pathway. While a simulation model has been constructed that describes this case, it is not included here because it does not improve the fit of the simulation to the experimental data.

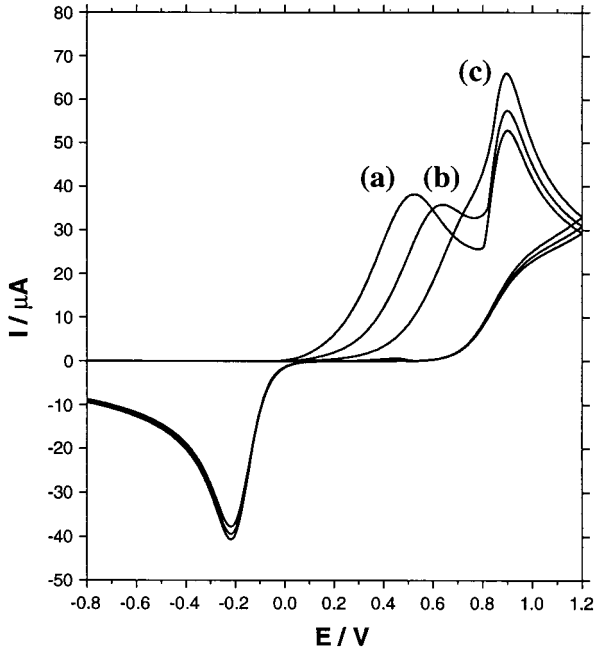

Figure 9. Simulated cyclic voltammograms for 10 mM solutions of McMT containing (a) 5 mM lutidine, (b) 5 mM Py, and (c) 5 mM 3-chloropyridine. Initial scan directions are all positive from -0.8 V. All other conditions as in Figure 8.

Conclusion

This study has described the influence of strong and weak bases on the oxidation of thiols and the influence of proton sources on the reductive cleavage of disulfides. A comparison of experimental data with simulations shows that a unique reaction pathway involving a proton transfer between the thiol and the weak base is important in the base facilitated oxidation of the thiols. It was postulated long ago that hydrogen bonding between amines and thiols might facilitate thiol oxidations.[36−38] However, as of yet there has been no detailed mechanistic study of this process. In particular, the notion of hydrogen-bonded complexes as key intermediates along the oxidation reaction pathway seems quite novel. This finding is in general agreement with expectations based on previous studies of the rapid proton transfer reactions involving acids of heteroatoms.[16−18,22,30,39] The importance of hydrogen bonding for redox processes occurring in nonaqueous solvents has been emphasized recently, especially with regard to the electrochemistry of quinones.[40]

These results also bear on the mechanism by which poly(aniline) facilitates the charge and discharge of DMcT in composite cathodes formed from mixtures of these materials.[1−7] Specifically, the finding that proton-accepting character can dramatically alter the rates and potentials for thiol oxidations, just as proton donor character can affect the reduction of disulfides to regenerate either thiols or thiolates, suggests that the action of poly(aniline) in these composite cathode systems probably involves such proton transfer character. This importance of proton transfer may have a detrimental impact on the use of poly(aniline) to catalyze the redox processes for thiolate/disulfide redox couples in Li secondary batteries due to the adverse affect of protons in such batteries.

Acknowledgment. This work was supported in full by the Office of Naval Research.

References and Notes

(1) Oyama, N.; Tatsuma, T.; Sato, T.; Sotomura, T. *Nature* **1995**, *373*, 598.
(2) Kaminaga, A.; Tatsuma, T.; Sotomura, T.; Oyama, N. *J. Electrochem. Soc.* **1995**, *142*, 47.
(3) Tatsuma, T.; Sotomura, T.; Sato, T.; Buttry, D. A.; Oyama, N. *J. Electrochem. Soc.* **1995**, *142*, L182.
(4) Shouji, E.; Matsui, H.; Oyama, N. *J. Electroanal. Chem.* **1996**, *417*, 17.
(5) Shouji, E.; Oyama, N. *J. Electroanal. Chem.* **1996**, *410*, 229.
(6) Tatsuma, T.; Matsui, H.; Shouji, E.; Oyama, N. *J. Phys. Chem.* **1996**, *100*, 14016.
(7) Shouji, E.; Yokoyama, Y.; Pope, J. M.; Oyama, N.; Buttry, D. A. *J. Phys. Chem. B* **1997**, *101*, 2861.
(8) Liu, M.; Visco, S. J.; De Jonghe, L. C. *J. Electrochem. Soc.* **1990**, *137*, 750.
(9) Murray, R. W. *Electroanalytical Chemistry*; Bard, A. J., Ed.; Marcel Dekker, Inc.: New York and Basel, 1984; Vol. 13, p 206.
(10) Daum, P.; Murray, R. W. *J. Phys. Chem.* **1981**, *85*, 389.
(11) Daum, P.; Murray, R. W. *J. Electroanal. Chem.* **1979**, *103*, 289.
(12) Simic, M.; Hoffman, M. Z. *J. Am. Chem. Soc.* **1970**, *92*, 6096.
(13) Hayon, E.; Hoffman, M. Z. *J. Am. Chem. Soc.* **1972**, *94*, 7950.
(14) Andrieux, C. P.; Saveant, J.; Tallec, A.; Tardivel, R.; Tardy, C. *J. Am. Chem. Soc.* **1997**, *119*, 2420.
(15) Bordwell, F. G. *Acc. Chem. Res.* **1988**, *21*, 456.
(16) Parker, V. D.; Tilset, M. *J. Am. Chem. Soc.* **1988**, *110*, 1649.
(17) Bordwell, F. G.; Bausch, M. J. *J. Am. Chem. Soc.* **1986**, *108*, 2473.
(18) Bordwell, F. G.; Cheng, J.-P. *J. Am. Chem. Soc.* **1989**, *111*, 1792.
(19) Parker, V. D.; Handoo, K. L.; Roness, F.; Tilset, M. *J. Am. Chem. Soc.* **1991**, *113*, 7493.
(20) Bordwell, F. G.; Zhang, X.-M.; Satish, A. V.; Cheng, J.-P. *J. Am. Chem. Soc.* **1994**, *116*, 6605.
(21) Bernasconi, C. F.; Carre, D. J. *J. Am. Chem. Soc.* **1979**, *101*, 2707.
(22) Parker, V. D.; Chao, Y.; Reitstöen, B. *J. Am. Chem. Soc.* **1991**, *113*, 2336.
(23) Rudolph, M. *Physical Electrochemistry: Principles, Methods and Applications*; Rubinstein, I., Ed.; Marcel Dekker: New York, 1994; Chapter 3, pp 81-130.
(24) Luo, W.; Feldberg, S. W.; Rudolph, M. *J. Electroanal. Chem.* **1994**, *368*, 109.
(25) Fry, A. J. *Topics in Organic Electrochemistry*; Fry, A. J.; Britton, W. E., Eds.; Plenum: New York, 1986; Chapter 1, pp 1−34.
(26) Shouji, E.; Buttry, D. A. *Langmuir* **1999**, *15*, 669.
(27) Laviron, E. *J. Electroanal. Chem.* **1986**, *208*, 357.
(28) March, J. *Advanced Organic Chemistry*; 4th ed.; Wiley: New York, 1992; p 250.
(29) Kolthoff, I. M.; Chantooni, M. K., Jr.; Bhowmik, S. *J. Am. Chem. Soc.* **1968**, *90*, 23.
(30) Schlesener, C. J.; Amatore, C.; Kochi, J. K. *J. Am. Chem. Soc.* **1984**, *106*, 7472.
(31) Observed ^{1}H NMR peaks for 3-chloropyridine in AN-d_3 were 7.32, 7.80, 8.51, and 8.63 ppm; those for 3-chloropyridine were 2.43 (methyl), 6.96, and 7.4; and those for 2,6-di-*tert*-butylpyridine were 1.37 (methyl), 7.15, and 7.58.
(32) Pyridine peaks in IR spectrum: 3082.8, 3001.9, 1582.3, 1439.1, 1374.8, 1217.5 cm^{-1}. Those for McMT: 3207.1, 2899.9, 1572.4, 1455.0, 1261.0, 1199.9 cm^{-1}. Those for McMT plus pyridine: 3207.2, 3082.8, 3001.9, 2898.1, 1582.2, 1454.1, 1439.2, 1261.1, 1200.1 cm^{-1}. The spectrum for McMT/pyridine mixtures was the summation of those for McMT and pyridine.
(33) Pyridine peaks in Raman spectrum: 1204.9, 1023.4, 982.4 cm^{-1}. Those for McMT: 1533.8, 1247.6, 1054.6, 660.3, 542.6, 440.8 cm^{-1}. Those for McMT plus pyridine: 1533.9, 1247.7, 1055.4, 1024.9. 983.9, 657.2, 441.5 cm^{-1}. The spectrum for McMT/pyridine mixtures was the summation of those for McMT and pyridine.
(34) Bard, A. J.; Faulkner, L. R. *Electrochemical Methods*; Wiley: New York, 1980; pp 450.
(35) IUPAC; *Ionization Constants of Organic Acids in Aqueous Solution*; Pergamon: New York, 1979.
(36) Gilman, H. *J. Am. Chem. Soc.* **1945**, *67*, 1845.
(37) Barnett, J. *J. Chem. Soc.* **1944**, 5.
(38) Gabriel, S.; Colman, J. *Ber.* **1912**, *45*, 1643.
(39) Nicholas, A. M.; Arnold, D. R. *Can. J. Chem.* **1982**, *60*, 2165.
(40) Gupta, N.; Linschitz, H. *J. Am. Chem. Soc.* **1997**, *119*, 6384.